Nonreciprocity with Structured Light Using Optical Pumping in Hot Atoms

Fei Song,[1] Zhiping Wang,[1,*] Enze Li,[2] Benli Yu,[1] and Zhixiang Huang[1,3]

[1] *Key Laboratory of Opto-Electronic Information Acquisition and Manipulation, Ministry of Education, Anhui University, Hefei 230601, China and Information Materials and Intelligent Sensing Laboratory of Anhui Province, Anhui University, Hefei 230601, China*

[2] *Key Laboratory of Quantum Information, University of Science and Technology of China, Hefei, Anhui 230026, China*

[3] *Key Laboratory of Intelligent Computing and Signal Processing, Ministry of Education, Anhui University, Hefei 230039, China*

(Received 16 November 2021; revised 2 April 2022; accepted 14 June 2022; published 9 August 2022)

Nonreciprocal transmission of structured light has possible applications in high-capacity optical communication and high-dimensional signal processing. Here, we demonstrate the magnet-free and cavity-free optical nonreciprocity of an orbital-angular-momentum (OAM) beam using optical-pumping technology with the assistance of the Doppler effect in hot atoms. By using optical pumping to induce a direction-dependent population transfer of the ground-state atoms, we realize optical nonreciprocity for the signal laser that is carrying OAM. Interestingly, an isolation ratio close to 30 dB and maximum transmission over 0.86 can be achieved simultaneously without the use of an optical cavity. Due to the unique amplitude and helical phase profile of the structured light, our proposal may open an avenue for exploring the singularity characteristics of optical nonreciprocity using structured light.

DOI: 10.1103/PhysRevApplied.18.024027

I. INTRODUCTION

Orbital-angular-momentum (OAM) light has been established as one of the most relevant and useful degrees of freedom of light [1], from both a fundamental [2] and an applied perspective [3], in the physical sciences [4–8]. The use of OAM modes, especially Laguerre-Gaussian (LG) beams, in classical [9–12] and quantum [13–21] areas has been extensively explored. However, the advantages of OAM modes have not yet been explored in hot atoms to realize optical nonreciprocity.

Optical nonreciprocity, which is known as a symmetry-breaking effect, has been widely studied due to its applications in signal processing and quantum networks [22–24]. Conventionally, the method of realizing optical nonreciprocity is based on the magneto-optical Faraday effect [25,26] but large magnetic fields are too bulky to be implemented on chip [27]. To avoid the above disadvantage, many magnet-free schemes for nonreciprocal light transport including spatiotemporal modulation [28–33] and nonlinear effects [34–38], as well as various other approaches [39–44] have attracted significant attention owing to their substantial ability to break the limit of the traditional Faraday effect. Recently, various strategies have also been pursued to break the optical reciprocity using hot atoms [45–51]. In particular, atomic thermal motion has been used in the discovery of strong nonreciprocity in the dynamics of chiral quantum systems modeled by creating susceptibility-momentum locking [52].

Despite the rapid developments in optical nonreciprocity in recent years, it is still challenging to efficiently realize optical nonreciprocity with an OAM beam in hot atoms due to the zero intensity at the core of such a beam. Here, we demonstrate the magnet-free and cavity-free optical nonreciprocity of an OAM beam using optical-pumping technology in hot atoms with the assistance of the Doppler effect. By using optical pumping to induce a direction-dependent population transfer of the ground-state atoms, we realize optical nonreciprocity for the signal laser that is carrying OAM. Interestingly, an isolation ratio close to 30 dB and maximum transmission over 0.86 can be achieved simultaneously without the use of an optical cavity. Compared with the previous studies [53–59], our proposal has three distinguishing features. First, our scheme realizes the magnet-free and cavity-free optical nonreciprocity of an OAM beam with a high isolation ratio and high transmission in hot atoms. Second, unlike the conventional Gaussian beam, an OAM beam represents a fundamentally different optical degree of freedom and provides unique optical properties, so our proposal may open an avenue for achieving structured nonreciprocal devices using an OAM beam. Third, optical nonreciprocal devices, such as optical

*Corresponding author. wzp@ahu.edu.cn

isolators, circulators, and phase shifts, are basic units of all-optical communications. Thus, structured nonreciprocal devices will have possible applications in high-capacity optical communications and high-dimensional signal processing.

II. THEORY AND EXPERIMENTAL METHODS

The inset in Fig. 1 shows the three-level V-type atomic system of the ^{85}Rb atom, which has one ground state $|1\rangle$ and two excited states $|2\rangle$ and $|3\rangle$. The designated states can be chosen as $|1\rangle = |5^2S_{1/2}, F = 2\rangle$, $|2\rangle = |5^2P_{1/2}, F = 3\rangle$, and $|3\rangle = |5^2P_{3/2}, F = 3\rangle$. The signal field Ω_s couples to the atomic transition $|5^2S_{1/2}, F = 2\rangle \leftrightarrow |5^2P_{3/2}, F = 3\rangle$ ($|1\rangle \leftrightarrow |3\rangle$) with a detuning Δ_s, while the pump field Ω_p drives the transition $|5^2S_{1/2}, F = 2\rangle \leftrightarrow |5^2P_{1/2}, F = 3\rangle$ ($|1\rangle \leftrightarrow |2\rangle$) with a detuning Δ_p. The signal field $\Omega_s = \Omega_0\Psi(r,z)e^{-il\phi}$ is a LG mode, where $\Psi(r,z) = \frac{\sqrt{2p!/\pi(p+|l|)!}}{\omega(z)}[\frac{\sqrt{2}r}{\omega(z)}]^{|l|}L_p^{|l|}[\frac{2r^2}{\omega^2(z)}]e^{\frac{-r^2}{\omega^2(z)}}e^{-i\Theta(r,z)}$, Ω_0 is the initial Rabi frequency of the signal field, $\Theta(r,z) = \tilde{k}r^2/2R(z) - (2p + |l| + 1)\tan^{-1} z/z_R$, $L_p^{|l|}$ is the Laguerre polynomial, z_R is the Rayleigh length for a given beam waist ω_0, $R(z) = z\left(1 + z^2/z_R^2\right)$ is the radius of curvature of the wave front, and $\omega(z) = \omega_0\left(1 + z^2/z_R^2\right)^{-1}$ and $(2p + |l| + 1)\tan^{-1} z/z_R$ describe the beam expansion and the Gouy phase accumulated during the diffraction propagation, respectively. $r = \sqrt{x^2 + y^2}$ is the radial radius, l is the topological charge, ϕ is the azimuthal angle, and p denotes the number of radial nodes in the mode profile. The wave numbers of the signal field and pump field are denoted by k_s and k_p, respectively. Because of the Doppler effect of atoms, the signal and pump beams are both subject to a direction-dependent Doppler frequency shift seen by the hot atoms. Taking into account the random thermal motion of atoms with v, the detunings change into $(\Delta_s + k_s v,\ \Delta_p + k_p v)$ for the copropagating case and $(\Delta_s - k_s v,\ \Delta_p + k_p v)$ for the counterpropagating case. In the interaction picture and under the rotating-wave approximation, the Hamiltonians for the copropagating and counterpropagating cases are given by

$$H_{\rm co} = -(\Delta_p + k_p v)\sigma_{22} - (\Delta_s + k_s v)\sigma_{33} + \frac{1}{2}(\Omega_p\sigma_{12} + \Omega_s^{+}\sigma_{13} + \text{H.c.}), \tag{1a}$$

$$H_{\rm cou} = -(\Delta_p + k_p v)\sigma_{22} - (\Delta_s - k_s v)\sigma_{33} + \frac{1}{2}(\Omega_p\sigma_{12} + \Omega_s^{-}\sigma_{13} + \text{H.c.}), \tag{1b}$$

where $\sigma_{ij} = |i\rangle\langle j|\,(i,j = 1,2,3)$ are the atomic transition operators and "H.c." represents the Hermitian conjugate. The frequency differences among the two lasers are quite small compared with their absolute frequencies; for simplicity, here we take $k_s \simeq k_p = k$. Ω_s^{+} is the signal field for the copropagating case when the topological charge $l = 2$, while Ω_s^{-} is the signal field for the counterpropagating case when the topological charge $l = -2$.

The dynamics of this system can be described by utilizing the density-matrix approach as

$$\dot{\rho} = -\frac{i}{\hbar}[H_{\rm co/cou}, \rho] - \frac{1}{2}\{\Gamma, \rho\}, \tag{2}$$

where $\{\Gamma, \rho\} = \Gamma\rho + \rho\Gamma$.

By substituting the interaction Hamiltonians given by Eqs. (1a) and (1b) into Eq. (2), we can calculate the density-matrix elements $\rho_{13}^{\rm co}(\Delta_s + kv, \Delta_p + kv)$ and $\rho_{13}^{\rm cou}(\Delta_s - kv, \Delta_p + kv)$. The linear susceptibility of the medium for the weak signal-laser field is determined by the term $\rho_{13}^{\rm co/cou}$. Consequently, the susceptibilities for the copropagating and counterpropagating cases can be written as

$$\chi_{\rm co} = \int_x\int_y\int_v \frac{|\mu_{13}|^2}{2\hbar\varepsilon_0\Omega_s^{+}}N(v)\rho_{13}^{\rm co}dxdydv, \tag{3a}$$

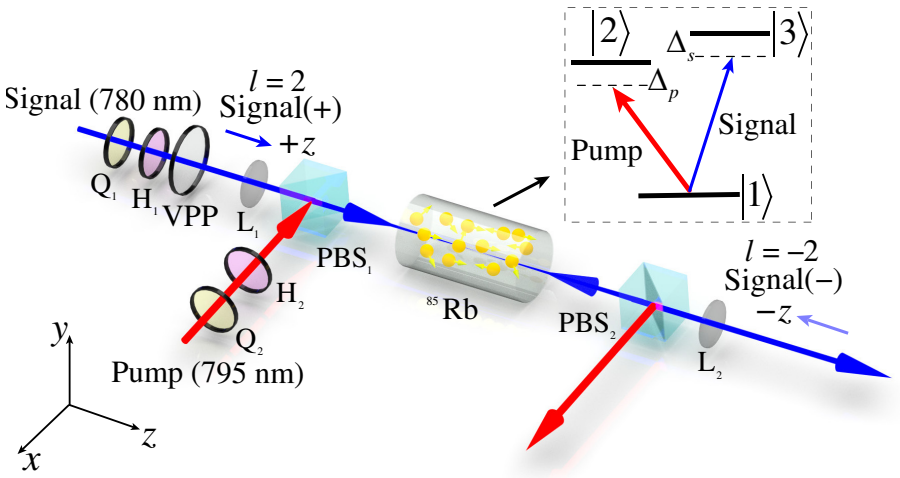

FIG. 1. The experimental setup for optical nonreciprocity of an OAM beam in hot ^{85}Rb atoms: Q_i $(i = 1,2)$, quarter-wave plate; H_j $(j = 1,2,3)$, half-wave plate; VPP, vortex phase plate; L_n $(n = 1,2)$, lens; PBS_k $(k = 1,2,3)$, polarizing beam splitter. The inset is a three-level atomic configuration.

$$\chi_{\rm cou} = \int_x \int_y \int_v \frac{|\mu_{13}|^2}{2\hbar\varepsilon_0\Omega_s^-} N(v)\rho_{13}^{\rm cou} dxdydv, \qquad (3b)$$

where $N(v) = N\exp(-v^2/u^2)/(u\sqrt{\pi})$ is the Maxwell-Boltzmann velocity distribution with N being the atomic number density in the medium, ε_0 is the permittivity in free space, and μ_{13} is the transition dipole moment between states $|1\rangle$ and $|3\rangle$. Here, $u = (2k_BT/m)^{1/2}$, which is the most probable atomic speed at temperature T, k_B is the Boltzmann constant, and m is the mass of the atom.

It is worth noting that the direction-dependent susceptibilities in Eqs. (3a) and (3b) induce the nonreciprocity. The transmission T_+ for the copropagating and T_- counterpropagating cases can be written as

$$T_+ = \exp\{-2{\rm Im}[(\omega_s/c)(1+\chi_{\rm co}/2)]L_e\}, \qquad (4a)$$

$$T_- = \exp\{-2{\rm Im}[(\omega_s/c)(1+\chi_{\rm cou}/2)]L_e\}, \qquad (4b)$$

where ω_s is the frequency of the signal field, c is the speed of light in vacuum, and L_e is the effective length of the vapor cell.

The experimental setup is shown in Fig. 1. The inset shows the three-level V-type atomic system of the ^{85}Rb atom. The signal and pump beams drive the transitions $|5^2S_{1/2}, F=2\rangle \leftrightarrow |5^2P_{3/2}, F=3\rangle$ ($|1\rangle \leftrightarrow |3\rangle$) and $|5^2S_{1/2}, F=2\rangle \leftrightarrow |5^2P_{1/2}, F=3\rangle$ ($|1\rangle \leftrightarrow |2\rangle$), respectively. A Gaussian beam with horizontal polarization (generated by a tunable diode laser, $\lambda = 780$ nm) is sent to a vortex phase plate (VPP) to generate the OAM signal(+) beam with the topological charge $l = 2$, while the signal(−) beam with the topological charge $l = -2$ can be generated via the signal(+) beam using a mirror. The pump beam (beam diameter 0.8 mm) is generated by a tunable diode laser working at 795 nm and later enhanced by a laser amplifier. The signal(+) beam [signal(−) beam] is focused by a lens L_1 ($f_1 = 30$ cm) [lens L_2 ($f_2 = 30$ cm)], transmitting a 50-mm-long natural-abundance Rb vapor cell to another lens L_2 ($f_2 = 30$ cm) [lens L_1 ($f_1 = 30$ cm)] and forming an image in the charge-coupled device (CCD) camera beam profiler. The transmission spectra of the signal(+)/signal(−) field can be detected by amplified photodetectors. In the copropagating case, the signal(+) and pump beams with vertical polarization directions almost copropagate and the angle between the two beams is about 1°. For the counterpropagating case, the signal(−) and pump beams almost counterpropagate and have vertical polarization directions.

III. RESULTS AND DISCUSSION

In Fig. 2(a), we present the experimental beam path for the copropagating case. Figures 2(a1) and 2(a2) show the intensity profile of the signal(+) beam before and after a VPP. A lens L_1 images the far field of the VPP onto the atoms and the intensity profile of the signal(+) beam at the atomic cell center is illustrated in Fig. 2(a3). Then, we turn on the pump field. The intensity profile of the signal(+) beam after absorption from the atoms can be further imaged onto a CCD camera [see Fig. 2(a4)]. However, when the signal(−) and pump beams counterpropagate

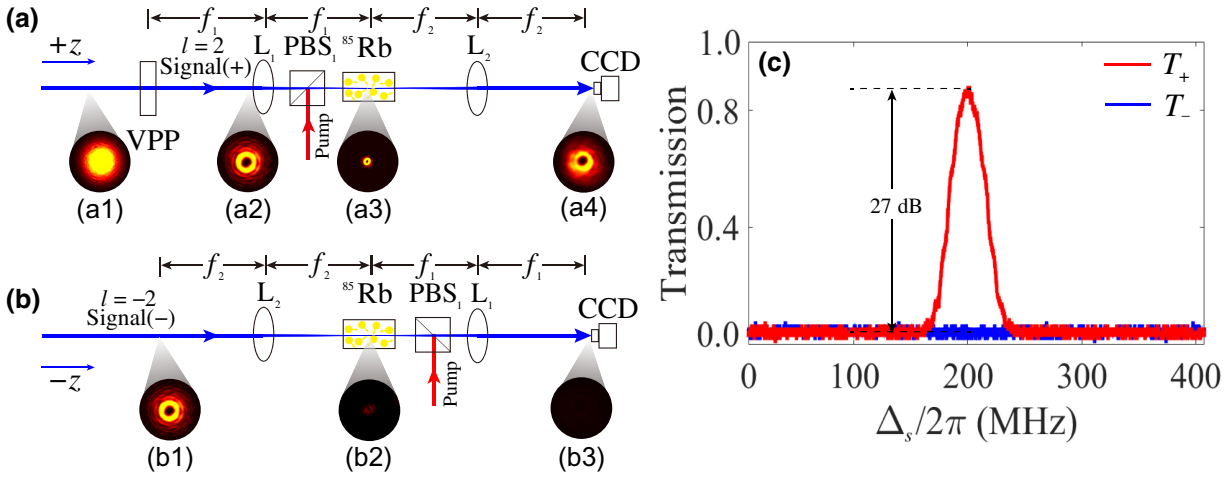

FIG. 2. (a) The experimental beam path for the copropagating case: (a1),(a2), the intensity profiles of the signal(+) beam before and after a VPP; (a3) the intensity profile of the signal(+) beam with a diameter of 0.2 mm at the atomic cell center; (a4) the intensity profile of the signal(+) beam after absorption from the atoms imaged onto the CCD camera. (b) The experimental beam path for the counterpropagating case: (b1) the intensity profile of the signal(−) beam; (b2) the intensity profile of the signal(−) beam with a diameter of 0.2 mm at the atomic cell center; (b3) the intensity profile of the signal(−) beam after absorption from the atoms imaged onto the CCD camera. (c) Nonreciprocal transmission spectra of the signal field for copropagating (T_+, red line) and counterpropagating (T_-, blue line) cases versus its detuning Δ_s. Here, the signal-field power is fixed at 10μW, the pump-field power is fixed at 40 mW, the temperature of the atomic cell is set at 55 °C, and the detuning of the pump field is $\Delta_p = 2\pi \times 200$ MHz.

with vertical polarization directions in the counterpropagating case, with the experimental beam path as displayed in Fig. 2(b), there is no intensity profile of the signal beam imaged onto the CCD camera [see Fig. 2(b3)]. Evidently, by reversing the signal direction, we realize optical nonreciprocity for the signal laser that is carrying OAM. For an understanding of the above phenomena, we show the typical nonreciprocal transmission spectra of the signal field versus its detuning Δ_s in Fig. 2(c). From this figure, we can see that the signal field exhibits a high transmittance in the copropagating case (T_+, red line), while it is strongly absorbed in the counterpropagating case (T_-, blue line) at the position $\Delta_s = 2\pi \times 200$ MHz, and the isolation ratio is 27 dB. The above results can be qualitatively explained as follows. For the copropagating case, the condition $\Delta_p = vk_p$ is met—namely, the pump field resonates with the group of atoms with velocity $v = \Delta_p/k_p$. Thus, the ground-state atoms are transferred, leading to a high transmission for the signal field around the position $\Delta_s = \Delta_p k_s/k_p = 2\pi \times 200$ MHz. In contrast, the pump field "seen" by the atoms with velocity $-v$ for the counterpropagating case is far from resonance. It can hardly pump the atoms away from the ground state and therefore the signal field is still strongly absorbed around the position

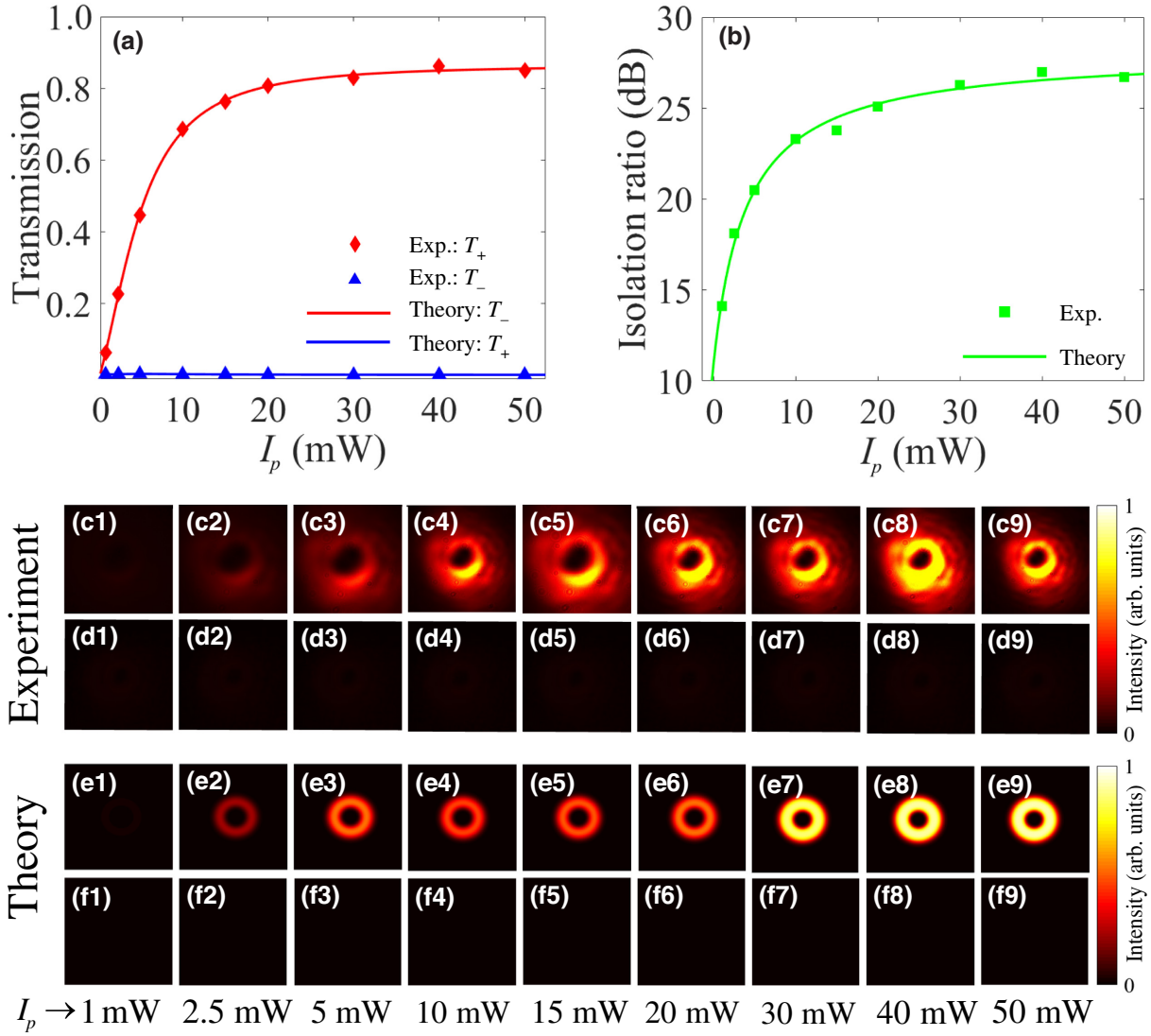

FIG. 3. (a) The nonreciprocal transmission spectra of the signal field for copropagating (T_+, red line) and counterpropagating (T_-, blue line) cases versus the pump-field power I_p. The other parameters are the same as in Fig. 2(c). (b) The isolation ratio as a function of the pump-field power I_p. (c1)–(c9) and (d1)–(d9) are the experimental intensity profiles of the signal field for the copropagating and counterpropagating cases with different pump-field powers I_p. (e1)–(e9) and (f1)–(f9) are the corresponding numerical intensity profiles of the signal field. The parameters for the numerical results are $\Omega_0 = 2\pi \times 0.5$ MHz, $p = 0$, $|l| = 2$, $\omega_0 \approx 0.2$ mm, $\mu_{12} = 1.29 \times 10^{-29}$ C m, $L_e = 50$ mm, $\mu_{13} = 1.15 \times 10^{-29}$ C m, $\Delta_s \simeq \Delta_p = 2\pi \times 200$ MHz, $N \approx 2.2 \times 10^{17}$ m^{-3}, and $T = 55\,^{\circ}$C.

$\Delta_s = \Delta_p k_s/k_p = 2\pi \times 200$ MHz. In fact, the findings reveal that the direction-dependent population transfer of the ground-state atoms leads to the nonreciprocal transmission of the signal field.

Figure 3(a) depicts the signal-field transmission spectra for the copropagating and counterpropagating settings at different pump-field powers I_p. Clearly, the signal(+) field transmission is very sensitive to the pump-field power in the copropagating case, while the effect of the pump-field power on the transmission of the signal(−) beam is very limited in the counterpropagating case. In fact, by using optical pumping to induce a direction-dependent population transfer of the ground-state atoms, which can transmit or isolate the signal field depending on the propagation direction of the signal field, it can then be used for the optical isolator with OAM light. In Fig. 3(b), we plot the isolation ratio as a function of the pump-field power. As can be clearly noted in Fig. 3(b), the isolation ratio is modulated, which is close to 30 dB by an appropriate choice of the pump-field power. In order to inspect the influence of the pump field on the signal-field transmission, Figs. 3(c1)–3(c9) and Figs. 3(d1)–3(d9) show the experimental intensity profiles of the signal field versus different values of the pump-field power for the copropagating and

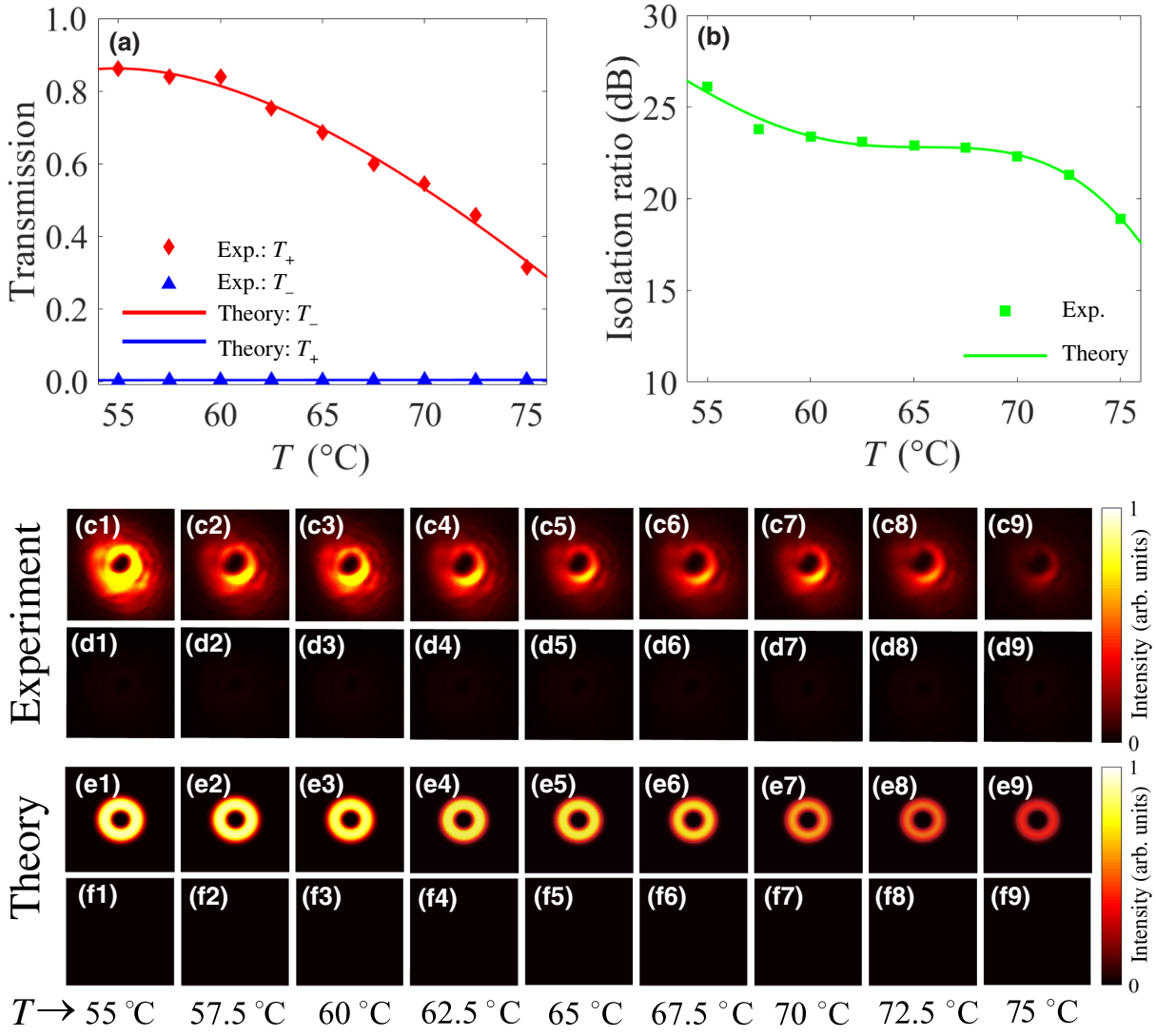

FIG. 4. (a) The nonreciprocal transmission spectra of the signal field for copropagating (T_+, red line) and counterpropagating (T_-, blue line) cases versus the temperature T of the atomic cell. The other parameters are the same as in Fig. 2(c). (b) The isolation ratio as a function of the temperature T of the atomic cell. (c1)–(c9) and (d1)–(d9) are the experimental intensity profiles of the signal field for the copropagating and counterpropagating cases with different temperatures T. (e1)–(e9) and (f1)–(f9) are the corresponding numerical intensity profiles of the signal field. The parameters for the numerical results are $\Omega_0 = 2\pi \times 0.5$ MHz, $\Omega_p = 2\pi \times 94$ MHz, $p = 0$, $|l| = 2$, $\omega_0 \approx 0.2$ mm, $\mu_{12} = 1.29 \times 10^{-29}$ C m, $L_e = 50$ mm, $\mu_{13} = 1.15 \times 10^{-29}$ C m, $\Delta_s \simeq \Delta_p = 2\pi \times 200$ MHz, and $N \approx 2.2 \times 10^{17}$ m^{-3} ($T = 55$ °C) and increase to 1.1×10^{18} m^{-3} for $T = 75$°C.

counterpropagating cases. As illustrated in these figures, by increasing the pump field, the intensity of the signal(+) field increases remarkably, so we can see that the signal(+) field transmission is increasing for the copropagating case. By contrast, for the counterpropagating case, there is no intensity profile of the signal(−) beam imaged onto the CCD camera. Meanwhile, the corresponding numerical intensity profiles of the signal(+)/signal(−) field are given in Figs. 3(e1)–3(e9) and Figs. 3(f1)–3(f9) and are in good agreement with our experimental results.

Finally, we present the measured signal-beam transmission spectra for different cell temperatures T in Fig. 4(a). When we increase the temperature of the cell from 55 °C to 75 °C, it is observed that the signal(−) field transmission for the counterpropagating case stays unchanged, while the transmission for the copropagating case drops strongly, from 0.86 to 0.32. To understand the above result, we note that an increase in temperature results in more frequent collisions and hence more severe decoherence for excited-state atoms, thereby causing the low pumping efficiency. Similarly, we give the isolation ratio as a function of the temperature T in Fig. 4(b). As shown in this figure, the isolation ratio obviously decreases with the increasing temperature T. Moreover, the experimental intensity distributions of the signal field versus different values of the temperature T for the copropagating and counterpropagating cases are shown in Figs. 4(c1)–4(c9) and Figs. 4(d1)–4(d9). As expected, with an increase of the cell temperature T, the intensity of the signal(+) field decreases remarkably for the copropagating case but we cannot probe the intensity profile of the signal(−) beam on the CCD camera for the counterpropagating case. The corresponding theoretical results are also given in Figs. 4(e1)–4(e9) and Figs. 4(f1)–4(f9), which readily verify the above experimental findings.

Before ending this section, it is worthwhile to briefly discuss two recent schemes for the realization of optical nonreciprocity with thermal atoms at room temperature [50,52]. In these two schemes, a three-level ladder-type or Lambda-type atomic system is used to manipulate the magnet-free nonreciprocity. Compared with these two schemes, the major characteristics of our proposal are the following. First, the main difference between our scheme and those in Refs. [50,52] is that we utilize an OAM beam, while in Refs. [50,52] only traditional beams are used. The OAM beam, unlike a conventional beam, is characterized by a helical wave front and has a more complex spatial distribution, which is nowadays an interesting resource in classical and quantum optics. For example, multiplexing is crucial for the data-carrying capacity of information communication systems and OAM with a topological charge l provides a degree of freedom to realize multiplexing. Second, it is worth noting that our approach is essentially different from the typical nonreciprocity electromagnetically induced transparency (EIT) effect [50,52]. The EIT effect takes advantage of the coherence of atoms but our mechanism makes use of optical-pumping technology with the assistance of the Doppler effect and the atomic collisions strongly destroy the atomic coherence. Third, our scheme can lead to higher transmission with low pump-field power. In our scheme, the maximum transmission is over 0.86, which is much higher than the transmission (approximately 0.638) in Ref. [50] based on the EIT effect in the single-photon regime. In addition, we simultaneously demonstrate a high isolation ratio and a low insertion loss for cavity-free optical nonreciprocity of the OAM beam, which is also a characteristic that the previous study [52] does not have.

IV. CONCLUSIONS

In conclusion, we propose a scheme to realize the magnet-free and cavity-free optical nonreciprocity of an OAM beam using optical-pumping technology in hot atoms with the assistance of the Doppler effect. By using optical pumping to induce a direction-dependent population transfer of the ground-state atoms, we realize optical nonreciprocity for the signal laser that is carrying OAM. Interestingly, an isolation ratio reaching nearly 30 dB and maximum transmission over 0.86 can be achieved simultaneously without the use of an optical cavity. Due to the richness of properties that OAM beams show under propagation, in focusing, and in their interaction with matter, our work may pave the way for the realization of high-dimensional optical nonreciprocal devices and provide opportunities for applications in high-capacity optical communication [60].

ACKNOWLEDGMENTS

We are indebted to Professor Baosen Shi (University of Science and Technology of China, USTC) for fruitful discussions and comments about this work. The work was supported by the National Natural Science Foundation of China (Grant No. 11674002).

[1] L. Allen, M. W. Beijersbergen, R. J. C. Spreeuw, and J. P. Woerdman, Orbital angular momentum of light and the transformation of Laguerre-Gaussian laser modes, Phys. Rev. A **45**, 8185 (1992).
[2] M. Padgett, J. Courtial, and L. Allen, Light's orbital angular momentum, Phys. Today **57**, 35 (2004).
[3] A. Forbes, M. de Oliveira, and M. R. Dennis, Structured light, Nat. Photonics **15**, 253 (2021).
[4] G. Molina-Terriza, J. P. Torres, and L. Torner, Twisted photons, Nat. Phys. **3**, 305 (2007).
[5] S. Franke-Arnold, L. Allen, and M. Padgett, Advances in optical angular momentum, Laser Photonics Rev. **2**, 299 (2008).

[6] M. Lassen, G. Leuchs, and U. L. Andersen, Continuous Variable Entanglement and Squeezing of Orbital Angular Momentum States, Phys. Rev. Lett. **102**, 163602 (2009).

[7] J. Leach, B. Jack, J. Romero, A. K. Jha, A. M. Yao, S. Franke-Arnold, D. G. Ireland, R. W. Boyd, S. M. Barnett, and M. J. Padgett, Quantum correlations in optical angle–orbital angular momentum variables, Science **329**, 662 (2010).

[8] X. Pan, S. Yu, Y. Zhou, K. Zhang, K. Zhang, S. Lv, S. Li, W. Wang, and J. Jing, Orbital-Angular-Momentum Multiplexed Continuous-Variable Entanglement from Four-Wave Mixing in Hot Atomic Vapor, Phys. Rev. Lett. **123**, 070506 (2019).

[9] A. M. Marino, V. Boyer, R. C. Pooser, P. D. Lett, K. Lemons, and K. M. Jones, Delocalized Correlations in Twin Light Beams with Orbital Angular Momentum, Phys. Rev. Lett. **101**, 093602 (2008).

[10] J. Wang, J.-Y. Yang, I. M. Fazal, N. Ahmed, Y. Yan, H. Huang, Y. Ren, Y. Yue, S. Dolinar, M. Tur, and A. E. Willner, Terabit free-space data transmission employing orbital angular momentum multiplexing, Nat. Photonics **6**, 488 (2012).

[11] N. Bozinovic, Y. Yue, Y. Ren, M. Tur, P. Kristensen, H. Huang, A. E. Willner, and S. Ramachandran, Terabit-scale orbital angular momentum mode division multiplexing in fibers, Science **340**, 1545 (2013).

[12] K. Y. Bliokh and F. Nori, Transverse and longitudinal angular momenta of light, Phys. Rep. **592**, 1 (2015).

[13] K. Liu, J. Guo, C. Cai, S. Guo, and J. Gao, Experimental Generation of Continuous-Variable Hyperentanglement in an Optical Parametric Oscillator, Phys. Rev. Lett. **113**, 170501 (2014).

[14] X.-L. Wang, X.-D. Cai, Z.-E. Su, M.-C. Chen, D. Wu, L. Li, N.-L. Liu, C.-Y. Lu, and J.-W. Pan, Quantum teleportation of multiple degrees of freedom of a single photon, Nature **518**, 516 (2015).

[15] Z.-Q. Zhou, Y.-L. Hua, X. Liu, G. Chen, J.-S. Xu, Y.-J. Han, C.-F. Li, and G.-C. Guo, Quantum Storage of Three-Dimensional Orbital-Angular-Momentum Entanglement in a Crystal, Phys. Rev. Lett. **115**, 070502 (2015).

[16] M. Malik, M. Erhard, M. Huber, M. Krenn, R. Fickler, and A. Zeilinger, Multi-photon entanglement in high dimensions, Nat. Photonics **10**, 248 (2016).

[17] W. Zhang, D.-S. Ding, M.-X. Dong, S. Shi, K. Wang, S.-L. Liu, Y. Li, Z.-Y. Zhou, B.-S. Shi, and G.-C. Guo, Experimental realization of entanglement in multiple degrees of freedom between two quantum memories, Nat. Commun. **7**, 1 (2016).

[18] A. Sit, F. Bouchard, R. Fickler, J. Gagnon-Bischoff, H. Larocque, K. Heshami, D. Elser, C. Peuntinger, K. Günthner, B. Heim, C. Marquardt, G. Leuchs, R. W. Boyd, and E. Karimi, High-dimensional intracity quantum cryptography with structured photons, Optica **4**, 1006 (2017).

[19] T.-M. Zhao, Y. S. Ihn, and Y.-H. Kim, Direct Generation of Narrow-Band Hyperentangled Photons, Phys. Rev. Lett. **122**, 123607 (2019).

[20] S. Li, X. Pan, Y. Ren, H. Liu, S. Yu, and J. Jing, Deterministic Generation of Orbital-Angular-Momentum Multiplexed Tripartite Entanglement, Phys. Rev. Lett. **124**, 083605 (2020).

[21] Y. Chen, S. Liu, Y. Lou, and J. Jing, Orbital Angular Momentum Multiplexed Quantum Dense Coding, Phys. Rev. Lett. **127**, 093601 (2021).

[22] H. J. Kimble, The quantum Internet, Nature **453**, 1023 (2008).

[23] D. Jalas, A. Petrov, M. Eich, W. Freude, S. Fan, Z. Yu, R. Baets, M. Popović, A. Melloni, J. D. Joannopoulos, M. Vanwolleghem, C. R. Doerr, and H. Renner, What is—and what is not—an optical isolator, Nat. Photonics **7**, 579 (2013).

[24] P. Lodahl, S. Mahmoodian, S. Stobbe, A. Rauschenbeutel, P. Schneeweiss, J. Volz, H. Pichler, and P. Zoller, Chiral quantum optics, Nature **541**, 473 (2017).

[25] Z. Wang, Y. Chong, J. D. Joannopoulos, and M. Soljačić, Observation of unidirectional backscattering-immune topological electromagnetic states, Nature **461**, 772 (2009).

[26] A. B. Khanikaev, S. H. Mousavi, G. Shvets, and Y. S. Kivshar, One-Way Extraordinary Optical Transmission and Nonreciprocal Spoof Plasmons, Phys. Rev. Lett. **105**, 126804 (2010).

[27] L. Bi, J. Hu, P. Jiang, D. H. Kim, G. F. Dionne, L. C. Kimerling, and C. Ross, On-chip optical isolation in monolithically integrated non-reciprocal optical resonators, Nat. Photonics **5**, 758 (2011).

[28] Z. Yu and S. Fan, Complete optical isolation created by indirect interband photonic transitions, Nat. Photonics **3**, 91 (2009).

[29] L. Feng, M. Ayache, J. Huang, Y.-L. Xu, M.-H. Lu, Y.-F. Chen, Y. Fainman, and A. Scherer, Nonreciprocal light propagation in a silicon photonic circuit, Science **333**, 729 (2011).

[30] K. Fang, Z. Yu, and S. Fan, Realizing effective magnetic field for photons by controlling the phase of dynamic modulation, Nat. Photonics **6**, 782 (2012).

[31] D. L. Sounas and A. Alu, Non-reciprocal photonics based on time modulation, Nat. Photonics **11**, 774 (2017).

[32] E. A. Kittlaus, N. T. Otterstrom, P. Kharel, S. Gertler, and P. T. Rakich, Non-reciprocal interband Brillouin modulation, Nat. Photonics **12**, 613 (2018).

[33] E. A. Kittlaus, W. M. Jones, P. T. Rakich, N. T. Otterstrom, R. E. Muller, and M. Rais-Zadeh, Electrically driven acousto-optics and broadband non-reciprocity in silicon photonics, Nat. Photonics **15**, 43 (2021).

[34] L. Fan, J. Wang, L. T. Varghese, H. Shen, B. Niu, Y. Xuan, A. M. Weiner, and M. Qi, An all-silicon passive optical diode, Science **335**, 447 (2012).

[35] A. B. Khanikaev and A. Alu, Nonlinear dynamic reciprocity, Nat. Photonics **9**, 359 (2015).

[36] Y. Shi, Z. Yu, and S. Fan, Limitations of nonlinear optical isolators due to dynamic reciprocity, Nat. Photonics **9**, 388 (2015).

[37] D. L. Sounas, J. Soric, and A. Alu, Broadband passive isolators based on coupled nonlinear resonances, Nat. Electronics **1**, 113 (2018).

[38] X. Guo, Y. Ding, Y. Duan, and X. Ni, Nonreciprocal metasurface with space-time phase modulation, Light Sci. Appl. **8**, 1 (2019).

[39] C.-H. Dong, Z. Shen, C.-L. Zou, Y.-L. Zhang, W. Fu, and G.-C. Guo, Brillouin-scattering-induced transparency and non-reciprocal light storage, Nat. Commun. **6**, 1 (2015).

[40] J. Kim, M. C. Kuzyk, K. Han, H. Wang, and G. Bahl, Non-reciprocal Brillouin scattering induced transparency, Nat. Phys. **11**, 275 (2015).

[41] Z. Shen, Y.-L. Zhang, Y. Chen, C.-L. Zou, Y.-F. Xiao, X.-B. Zou, F.-W. Sun, G.-C. Guo, and C.-H. Dong, Experimental realization of optomechanically induced non-reciprocity, Nat. Photonics **10**, 657 (2016).

[42] K. Fang, J. Luo, A. Metelmann, M. H. Matheny, F. Marquardt, A. A. Clerk, and O. Painter, Generalized non-reciprocity in an optomechanical circuit via synthetic magnetism and reservoir engineering, Nat. Phys. **13**, 465 (2017).

[43] N. R. Bernier, L. D. Toth, A. Koottandavida, M. A. Ioannou, D. Malz, A. Nunnenkamp, A. Feofanov, and T. Kippenberg, Nonreciprocal reconfigurable microwave optomechanical circuit, Nat. Commun. **8**, 1 (2017).

[44] R. Huang, A. Miranowicz, J.-Q. Liao, F. Nori, and H. Jing, Nonreciprocal Photon Blockade, Phys. Rev. Lett. **121**, 153601 (2018).

[45] K. Xia, F. Nori, and M. Xiao, Cavity-Free Optical Isolators and Circulators Using a Chiral Cross-Kerr Nonlinearity, Phys. Rev. Lett. **121**, 203602 (2018).

[46] G. Lin, S. Zhang, Y. Hu, Y. Niu, J. Gong, and S. Gong, Nonreciprocal Amplification with Four-Level Hot Atoms, Phys. Rev. Lett. **123**, 033902 (2019).

[47] C. Liang, B. Liu, A.-N. Xu, X. Wen, C. Lu, K. Xia, M. K. Tey, Y.-C. Liu, and L. You, Collision-Induced Broadband Optical Nonreciprocity, Phys. Rev. Lett. **125**, 123901 (2020).

[48] E.-Z. Li, D.-S. Ding, Y.-C. Yu, M.-X. Dong, L. Zeng, W.-H. Zhang, Y.-H. Ye, H.-Z. Wu, Z.-H. Zhu, W. Gao, G.-C. Guo, and B.-S. Shi, Experimental demonstration of cavity-free optical isolators and optical circulators, Phys. Rev. Res. **2**, 033517 (2020).

[49] S. Zhang, G. Lin, Y. Hu, Y. Qi, Y. Niu, and S. Gong, Cavity-Free Circulator with Low Insertion Loss Using Hot Atoms, Phys. Rev. Appl. **14**, 024032 (2020).

[50] M.-X. Dong, K.-Y. Xia, W.-H. Zhang, Y.-C. Yu, Y.-H. Ye, E.-Z. Li, L. Zeng, D.-S. Ding, B.-S. Shi, G.-C. Guo, and F. Nori, All-optical reversible single-photon isolation at room temperature, Sci. Adv. **7**, eabe8924 (2021).

[51] X. Lu, W. Cao, W. Yi, H. Shen, and Y. Xiao, Nonreciprocity and Quantum Correlations of Light Transport in Hot Atoms via Reservoir Engineering, Phys. Rev. Lett. **126**, 223603 (2021).

[52] S. Zhang, Y. Hu, G. Lin, Y. Niu, K. Xia, J. Gong, and S. Gong, Thermal-motion-induced non-reciprocal quantum optical system, Nat. Photonics **12**, 744 (2018).

[53] C. Sayrin, C. Junge, R. Mitsch, B. Albrecht, D. O'Shea, P. Schneeweiss, J. Volz, and A. Rauschenbeutel, Nanophotonic Optical Isolator Controlled by the Internal State of Cold Atoms, Phys. Rev. X **5**, 041036 (2015).

[54] B. He, L. Yang, X. Jiang, and M. Xiao, Transmission Nonreciprocity in a Mutually Coupled Circulating Structure, Phys. Rev. Lett. **120**, 203904 (2018).

[55] Y. Hu, S. Zhang, Y. Qi, G. Lin, Y. Niu, and S. Gong, Multiwavelength Magnetic-Free Optical Isolator by Optical Pumping in Warm Atoms, Phys. Rev. Appl. **12**, 054004 (2019).

[56] P. Yang, X. Xia, H. He, S. Li, X. Han, P. Zhang, G. Li, P. Zhang, J. Xu, Y. Yang, and T. Zhang, Realization of Nonlinear Optical Nonreciprocity on a Few-Photon Level Based on Atoms Strongly Coupled to an Asymmetric Cavity, Phys. Rev. Lett. **123**, 233604 (2019).

[57] X.-X. Hu, Z.-B. Wang, P. Zhang, G.-J. Chen, Y.-L. Zhang, G. Li, X.-B. Zou, T. Zhang, H. X. Tang, C.-H. Dong, G.-C. Guo, and C.-L. Zou, Noiseless photonic nonreciprocity via optically-induced magnetization, Nat. Commun. **12**, 1 (2021).

[58] S.-L. Ma, Y.-L. Ren, M.-T. Cao, S.-G. Zhang, and F.-L. Li, Optical isolator based on backward Brillouin scattering, Appl. Phys. Lett. **120**, 051109 (2022).

[59] L. Tang, J. Tang, M. Chen, F. Nori, M. Xiao, and K. Xia, Quantum Squeezing Induced Optical Nonreciprocity, Phys. Rev. Lett. **128**, 083604 (2022).

[60] A. E. Willner, K. Pang, H. Song, K. Zou, and H. Zhou, Orbital angular momentum of light for communications, Appl. Phys. Rev. **8**, 041312 (2021).